https://doi.org/10.1016/j.nanoen.2020.105549

Breathable, Washable and Wearable Woven-Structured Triboelectric Nanogenerators Utilizing Electrospun Nanofibers for Biomechanical Energy Harvesting and Self-Powered Sensing

Xiaoyang Guan, Bingang Xu*, Mengjie Wu, Titao Jing, Yujue Yang, Yuanyuan Gao

† Nanotechnology Center, Institute of Textiles and Clothing, The Hong Kong Polytechnic University, Hung Hom, Kowloon, Hong Kong, P. R. China

* Corresponding author. E-mail: tcxubg@polyu.edu.hk; Tel: +852-2766 4544

Abstract: With the rapid advancement in wearable electronics, energy harvesting devices based on triboelectric nanogenerators (TENGs) have been intensively investigated for providing sustainable power supply for them. However, the fabrication of wearable TENGs still remains great challenges, such as flexibility, breathability and washability. Here, a route to develop a new kind of woven-structured triboelectric nanogenerator (WS-TENG) with a facile, low-cost, and scalable electrospinning technique is reported. The WS-TENG is fabricated with commercial stainless-steel yarns wrapped by electrospun polyamide 66 nanofiber and poly(vinylidenefluoride-co-trifluoroethylene) nanofiber, respectively. Triggered by diversified friction materials under a working principle of freestanding mode, the open-circuit voltage, short-circuit current and maximum instantaneous power density from the WS-TENG can reach up to 166 V, 8.5 μA and 93 mW/m^2, respectively. By virtue of high flexibility, desirable breathability, washability and excellent durability, the fabricated WS-TENG is demonstrated to be a reliable power textile to light up 58 light-emitting diodes (LED) connected serially, charge commercial capacitors and drive portable electronics. A smart glove with stitched WS-TENGs is made to detect finger motion in different circumstances. The work presents a new approach for self-powered textiles with potential applications in biomechanical energy harvesting, wearable electronics and human motion monitoring.

Keywords: triboelectric nanogenerator; energy harvesting; electrospinning; wearable devices; human motion

1. Introduction

In recent years, flexible and wearable electronics have attracted tremendous interests owing to their widespread application potential in flexible circuits[1–3], wireless sensor networks[4–6], roll-up displays[7–9], healthcare monitoring[10–12], human-machine interface (HMI)[13,14], internet of things (IoTs)[15,16], artificial electronic skins (E-skins)[17–19] and so on. Meanwhile, with rapid advancement in wearable electronics, the demand for corresponding flexible and sustainable power supply units is continuously growing[20,21]. However, traditional chemical batteries, which are still the most widely used portable energy source so far, cannot meet the requirements of wearable electronics due to their inherent limitations of rigid complex structure, heavy weight, bulky volume, persistent recharging/replacement, and limited lifetime[22]. To address these challenges, one of the most promising solutions is to develop self-powered energy harvesters to scavenge waste biomechanical energy from human movements, which is ubiquitously available and can be generated continuously and inexhaustibly without ambient environment restriction[23,24]. To date, based on piezoelectric[25], electromagnetic[26], and triboelectric mechanisms[27–30], a variety of novel generators have been actively explored. Among them, the newly developed triboelectric nanogenerators (TENGs) with the advantages of simple configuration, light weight, high energy-conversion efficiency and flexibility in material selections, have become a burgeoning focus as the most promising candidates for efficiently harvesting biomechanical energy from various body motions[31–33]. TENGs are developed based on the coupling effects of triboelectrification and electrostatic induction, which causes charge transfer at the contact interface between two different materials with different electron affinities[34,35]. Up to now, numerous research endeavors have been committed to improve the performance of TENGs by a variety of approaches to broaden their application fields, which include selecting optimized friction materials[36,37], designing reasonable device structure[38,39], improving effective contact area[40], modifying surface structure[41,42] or chemical

compositions[43,44]. To develop high-performance TENGs, constructing micro/nanostructure on the surface of triboelectric materials has been demonstrated as an effective strategy to enlarge the friction area and enhance the triboelectric charge density[45]. However, commonly used techniques to design and fabricate micro/nanoarchitectures such as photolithography[46], nanoimprinting lithography[47], laser interference lithography[48] and reactive ion etching[49] are complicated, time-consuming and expensive. In this regard, manufacturing the surface micro/nanostructure of triboelectric materials with a simple, cost-effective and scalable fabrication method is still highly desired.

In comparison, electrospinning is a versatile, extremely simple and cost-effective technique to produce ultrathin fibers with a number of unique features and properties, including extraordinary length, large surface areas, hierarchically porous structures and intrinsically porosity[50,51]. In previous studies, electrospinning has already proved to be a suitable method in the field of TENGs for fabricating diverse membranes with nanofibrous surface microstructures from economically viable materials, such as nylon[52], poly (vinylidene fluoride) (PVDF)[53], polytetrafluoroethylene (PTFE)[54], ion gel[55] and so on. With the advantages of lightweight, softness and high porosity, nanofiber membranes are superior to dense film/rubber in wearable devices[56]. However, there still remain challenges for electrospun nanofiber based TENGs. First, most of the nanofiber-membrane-based TENGs have sandwich-like multilayer structure (including triboelectric layers, spacer, electrodes, supporting substrate, protective/ encapsulation layer, *etc.*), which are complicated to fabricate. Secondly, a majority of nanofiber-based TENGs need two individual triboelectric membranes to implement contact-separation motion, which limits the application of nanofiber-based TENGs. Thirdly, the materials used in the assembly of nanofiber based TENGs, including metal plate electrode, binder/tape, PET supporting substrate, silicone protective/encapsulation layer, seriously decrease the flexibility and breathability of the device. Finally, the multilayer planar structure cannot effectively sustain complex deformations caused by body movement, which is uncomfortable enough to be used in

wearable devices.

Herein, a novel nanofiber-based TENG with woven structure (WS-TENG) was introduced to address the issues mentioned above. The proposed WS-TENG was fabricated by using core-shell yarns composed of commercial stainless-steel yarn as the core and electrospun PA66 or P(VDF-TrFE) nanofibers as the shell through a simple electrospinning and scalable weaving method, which overcomes the complicated fabrication process, high cost, poor breathability, and discomfort of the previous reported nanofiber-based TENGs. Benefitting from the rational material pairs and surface nanostructure of nanofibers, a WS-TENG with the size of 5 × 5 cm^2 exhibits an excellent output open-circuit voltage with a peak-to-peak value of ~ 166 V, a short-circuit current of ~ 8.5 μA and a high instantaneous power density of ~ 93 mW/m^2 at a load resistance of 10 MΩ. With advantages of the all-fiber components, substrate-free, binder-free and interlaced woven structures, the WS-TENGs show high flexibility, desirable breathability, good washability and excellent durability. The prominent output power performance of WS-TENGs, together with combinatorial merits of nanofiber and textiles, makes them suitable for biomechanical energy harvesting and self-powered senor applications.

2. Experimental Section

2.1. Materials

PA66 (EPR-27) was purchased from Shenma Group Co., Ltd., China. P(VDF-TrFE) (Piezotech® FC25) was purchased from Arkema S.A., France. Stainless steel yarns (SSL, Bekaert Bekinox® VN AISI 316L) were purchased from N.V. Bekaert S.A., Belgium. Formic acid (88-91%, ACS reagent), *N, N*-Dimethylformamide (DMF, ≥99.8%, ACS reagent), acetone (≥99.5%, ACS reagent) and absolute alcohol (≥99.5%, ACS reagent) were purchased from Sigma-Aldrich. All the materials were used as received without any further purification. Copper/nickel-coated polyester fabric (CNF) were bought from the 3M company. Polytetrafluoroethylene (PTFE) film was provided by Jiangxi Aidmer Seal & Packing Co., Ltd., China. Plain-weave cotton fabric (120

g/m^2, yarn count: 40 S × 40 S) and polyester (PET) fabric (140 g/m^2, yarn count: 150 D × 150 D) were bought from a local textile company. The cotton fabric and PET fabric were cleaned with a commercial detergent aqueous solution and water successively before use.

2.2. Electrospinning

Prior to electrospinning, a solution of PA66 (15 wt %) was prepared by dissolving PA66 pellets in formic acid by continuous stirring for 2 h at a temperature of 70 ℃. Electrospinning process, schematically illustrated in Fig. 1a, was conducted on an electrospinning machine setup (TL-Pro, TONGLI Co. Ltd, China). During the electrospinning, a 10 mL plastic syringe with an 18 G metal nozzle was continuously fed by a syringe pump at a flow rate of 1 mL/h. Positive electrode of the high-voltage supply was connected to the metal nozzle, and a high voltage of around 25 kV with a distance of 25 cm between the nozzle tip and aluminum foil collector was applied. The aluminum foil collector was fixed on a rotating drum with diameter of 10 cm, which was rotated at a rate of 500 rpm, corresponding to a surface linear speed of 2.6 m/s. Environmental temperature and relative humidity were 22 ± 2 °C and 65 ± 5%, respectively. The electrospinning process was conducted for 4 h under the above-mentioned conditions. For fabrication of P(VDF-TrFE) nanofiber mat, P(VDF-TrFE) powders were firstly dissolved in a mixed solvent system of DMF and acetone with a weight ratio of 3:7 by magnetic stirring for 8 h at ambient temperature to obtain a 20 wt% solution of P(VDF-TrFE). Then, the electrospinning was carried out at a voltage of 25 kV over a distance of 14 cm from nozzle tip to the collector surface. All other experimental parameters and conditions were kept the same as stated above.

2.3. Fabrication of the WS-TENG

Stainless-steel yarns (SSY), with the advantages of excellent flexibility and high conductivity (210 S/cm), was suitable for serving as electrodes in wearable TENGs. Fig. 1b-f show the detailed manufacture process of the WS-TENG. Firstly, the electrospun PA66 nanofiber mat and P(VDF-TrFE) nanofiber mat were cut into strips

with dimension of 1 cm × 10 cm (Fig. 1b), and SSY was cut into short ones with a length of about 12 cm (Fig. 1c). Second, PA66 or P(VDF-TrFE) nanofiber strips were immersed into ethanol and wrapped onto the SSY to obtain PA66-SSY and P(VDF-TrFE)-SSY core-sheath yarns, respectively (Fig. 1d). Third, the prepared PA66-SSY and P(VDF-TrFE)-SSY core-sheath yarns were woven together to obtain a $M \times N$ woven structure textile (Fig. 1e), where M and N are the numbers of PA66-SSY and P(VDF-TrFE)-SSY core-sheath yarns, respectively. At last, all electrodes of the same core-sheath yarns were connected in parallel and a $M \times N$ WS-TENG was obtained (Fig. 1f). Fig. 1g shows a digital photo of a 60 × 60 WS-TENG.

2.4. Characterizations and measurements

The morphologies of the SSY, PA66-SSY and P(VDF-TrFE)-SSY core-sheath yarns were examined by scanning electron microscopy (SEM) (TESCAN VEGA3) operating at 20 kV, and the samples were coated with a thin layer of gold (around 2 nm) prior to the observation. The air permeability of the obtained WS-TENG was measured by Air Permeability Tester (SDL International M021S) according to standard (EN ISO 9237:2001). The water vapor transmission (WVT) rate of the obtained WS-TENG was tested according to the standard (GB/T 12704.1-2009). For comparison, commercial CNF, cotton and PET fabrics, which were used as friction materials, electrospun PA66 and P(VDF-TrFE) nanofiber mats, which served as friction layers, and a traditional sandwich-structured triboelectric nanogenerator (SS-TENG) using corresponding electrospun nanofibers were also tested, respectively. The electrical output performance of as-prepared WS-TENG under different applied forces and frequencies was evaluated on a Keyboard Life Tester (ZX-A03). The force signal was monitored by DAQ (Dewetron, Dewe-2600 DAQ system) at the same time. The open-circuit voltage and short-circuit current signals were recorded by an electrometer (Keithley 6514). For the washability measurement, WS-TENG were firstly washed for 20 min in a beaker containing 800 mL of aqueous detergent solution (1mg/ml) and a magnetic rotator (rotation speed: 200 rpm). Afterward, the WS-TENG was taken out and flushed with deionized water, dried in an oven at 80 C for 4 h and measured. The above-mentioned

washing and measurement processes were repeated 5 times.

3. Results and discussion

3.1. Design and fabrication of the WS-TENG

Fig.1a-f schematically illustrate the detailed construction process of the WS-TENG through electrospinning and traditional weaving technologies. Firstly, PA66 and P(VDF-TrFE) nanofiber mats were prepared by electrospinning (Fig.1a), respectively. Secondly, the nanofiber mats were cut into strips and wrapped onto SSY to obtain PA66-SSY and P(VDF-TrFE)-SSY core-sheath yarns (Fig.1b-d), respectively. Subsequently, a woven-structure textile was fabricated by weaving PA66-SSY as weft and P(VDF-TrFE) as warp with a handloom (Fig.1e). Finally, a WS-TENG was obtained by connecting all the electrodes of weft/warp yarns in parallel (Fig.1f).

Fig.1g shows a digital photo of a 60 × 60 WS-TENG with a dimension of about 5 cm × 5 cm. Owing to the softness of the electrospun nanofiber surface and the flexibility of SSY core electrodes, the WS-TENG maintains the advantages of comfort and biocompatibility. As shown in Fig.1h, the commercial two-ply SSY was used as the conductive electrode because of its excellent conductivity (210 S/cm), good flexibility and tactile comfort. Fig.1i-l show the SEM images of the P(VDF-TrFE)-SSY (Fig.1i-j) and PA66-SSY (Fig.1k-l) surface, respectively. Electrospun nanofiber layers were chosen as the dielectric material materials of the WS-TENG, owing to their nanofibrous surface microstructures, good softness, robust mechanical properties, excellent flexibility and good biocompatibility. According to the cross-section SEM images of P(VDF-TrFE)-SSY and PA66-SSY (insets of Fig.1i and k), the two-ply twisted SSY was approximately located in the center of core-sheath yarns, which suggests the uniform wrapping of nanofibers. In order to evaluate the flexibility of the fabricated yarns and WS-TENG device, flexibility measurements were conducted (as shown in Fig.S1 in the Supporting Information). As shown in Fig.S1 (a-f), both P(VDF-TrFE)-SSL and PA66-SSL yarns could be easily knotted without damaging the polymer nanofiber structures, suggesting their good flexibility. In addition, the fabricated WS-

TENG was capable of enduring various deformation states such as folding (Fig.S1g), rolling (Fig.S1h) and twisting (Fig.S1i), demonstrating its promising usability in wearable applications.

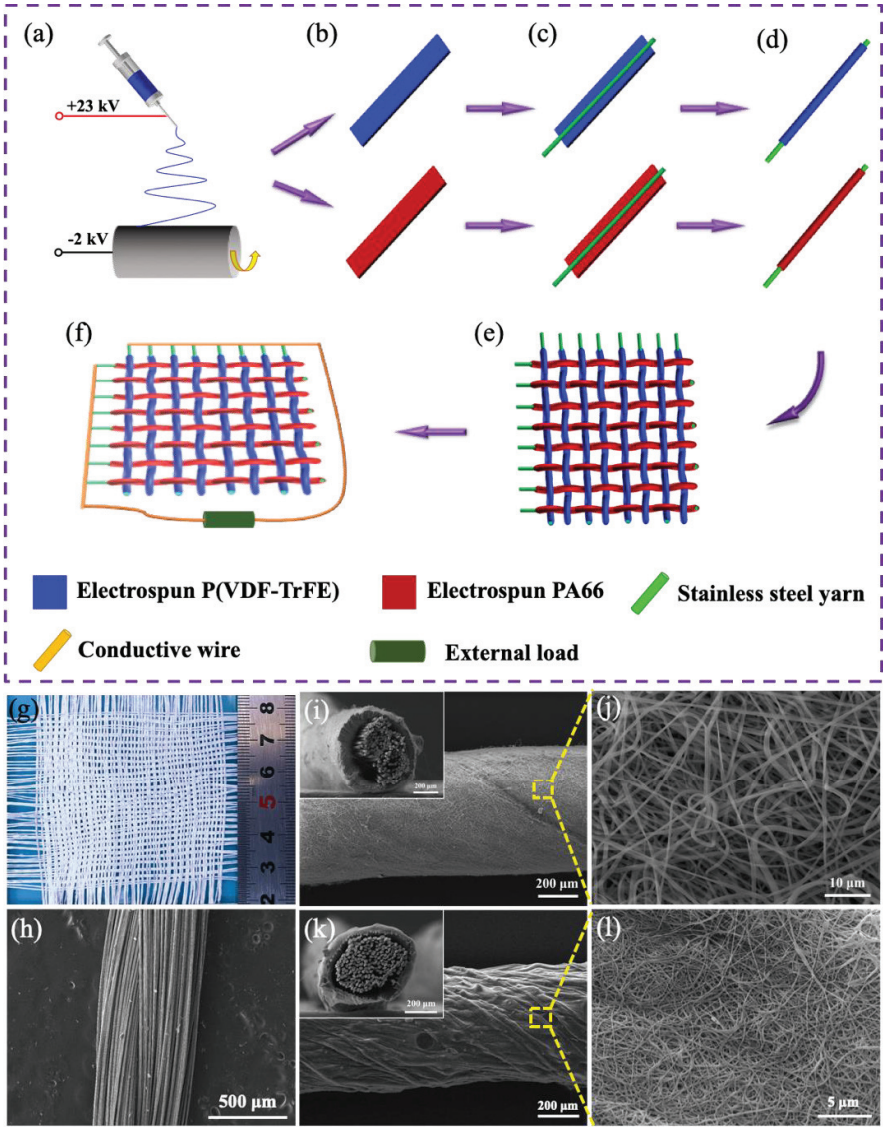

Fig. 1 (a-f) Fabrication process of the ESTENG. (g) Photographic image of the ESTENG. (h) SEM image of the SSL. SEM images of electrospun P(VDF-TrFE)/SSL surface at (i) low and (j) high magnifications; inset of (i) is the cross-section image. SEM images of electrospun PA66/SSL surface at (k) low and (l) high magnifications; inset of (k) is the cross-section image.

3.2. Working mechanism of the WS-TENG

In order to elucidate the power generation mechanism, working principle of the WS-

TENG is shown in Fig. 2a-f. Driven by a vertical impacting force, an external object (such as a rubber film) will periodically contact and separate from the WS-TENG (Fig.2a-b). Firstly, the freestanding rubber film is fully contacted with the WS-TENG under an applied force. Since the rubber film, P(VDF-TrFE) and PA66 have different electron affinities, the triboelectrification effect will render PA66 nanofiber surface with positive charges, while the part of rubber film that contacts with PA66 with negative charges. Meanwhile, P(VDF-TrFE) nanofiber surface will become negatively charged, and the part of rubber film that contacts with P(VDF-TrFE) is positively charged, as shown in Fig.2c. When the freestanding rubber film starts to move apart from the WS-TENG, an electric potential difference between PA66 and P(VDF-TrFE) layers is produced, which drives electrons to flow from the inner electrode of P(VDF-TrFE)-SSY to the inner electrode of PA66-SSY through an external circuit to equilibrate the triboelectric potential (Fig.2d). When the separation distance (*d*) between the freestanding rubber film and the WS-TENG increases to the maximum, a state of electrostatic equilibrium is reached and the electrons flowing is stopped (Fig. 2e). Subsequently, when the freestanding rubber film is driven to contact with the WS-TENG again, the former electrostatic equilibrium state is broken and then electrons flow back from the inner electrode of PA66-SSY to the inner electrode of P(VDF-TrFE)-SSY (Fig. 2f). When the freestanding rubber film moves to contact with the WS-TENG again, all of the induced charges become neutralized again (Fig.2c). As a result, a periodical alternating current signal can be generated under a freestanding-layer mode. Fig.2g-k demonstrate the versatility of WS-TENG in scavenging energy with different friction materials such as cotton fabric (Fig.2g), polyester fabric (Fig.2h), PTFE film (Fig.2i), CNF (Fig.2j) and rubber (Fig.2k).

3.3. Breathability

It is well known that breathability is one of the most important properties of wearable nanogenerator for various applications, which will influence the comfort of wearing such devices. As shown in Fig.2l, due to the low air permeability of CNF (38.3 ± 2.8 mm/s), electrospun PA66 mat (18.7 ± 1.5 mm/s) and P(VDF-TrFE) mat (23.2 ± 1.6),

the traditional sandwich-structured TENG (SS-TENG) showed inferior air permeability (12.4 ± 1.3 mm/s). While the obtained WS-TENG using corresponding electrospun PA66 and P(VDF-TrFE) mats exhibited excellent air permeability of 164 ± 5 mm/s, which was comparable with commercial cotton (103 ± 4 mm/s) and PET fabric (144 ± 5 mm/s). The measured results show that the WS-TENG is more suitable for wearable device when compared with the recently reported sandwich-like TENGs based on nanofibers.

In addition, water vapor permeability of the obtained WS-TENG, another key factor in breathability comfort of wearable devices, was also studied. As shown in Fig.2m, with the existence of interspace between the interlaced yarns, the water vapor permeability of the as-made WS-TENG was as high as 712 ± 16 g/m^2·24h, which was superior to commercial CNF (531 ± 17 g/m^2·24h), cotton (517 ± 18 g/m^2·24h) and PET fabrics (478 ± 15 g/m^2·24h). As expected, the corresponding SS-TENG had a much lower water permeability of 281 ± 14 g/m^2·24h due to the decreased moisture transmission of multilayers structure. Furthermore, compared with other nanofiber-based TENGs in the previous published works (shown in Table S1 in the Supporting Information), the developed WS-TENG also exhibits superior breathability. Therefore, it was believed that the new design idea of WS-TENG is more promising in comfort than recent sandwich-like nanofiber-based TENGs in self-powered wearable electronics applications.

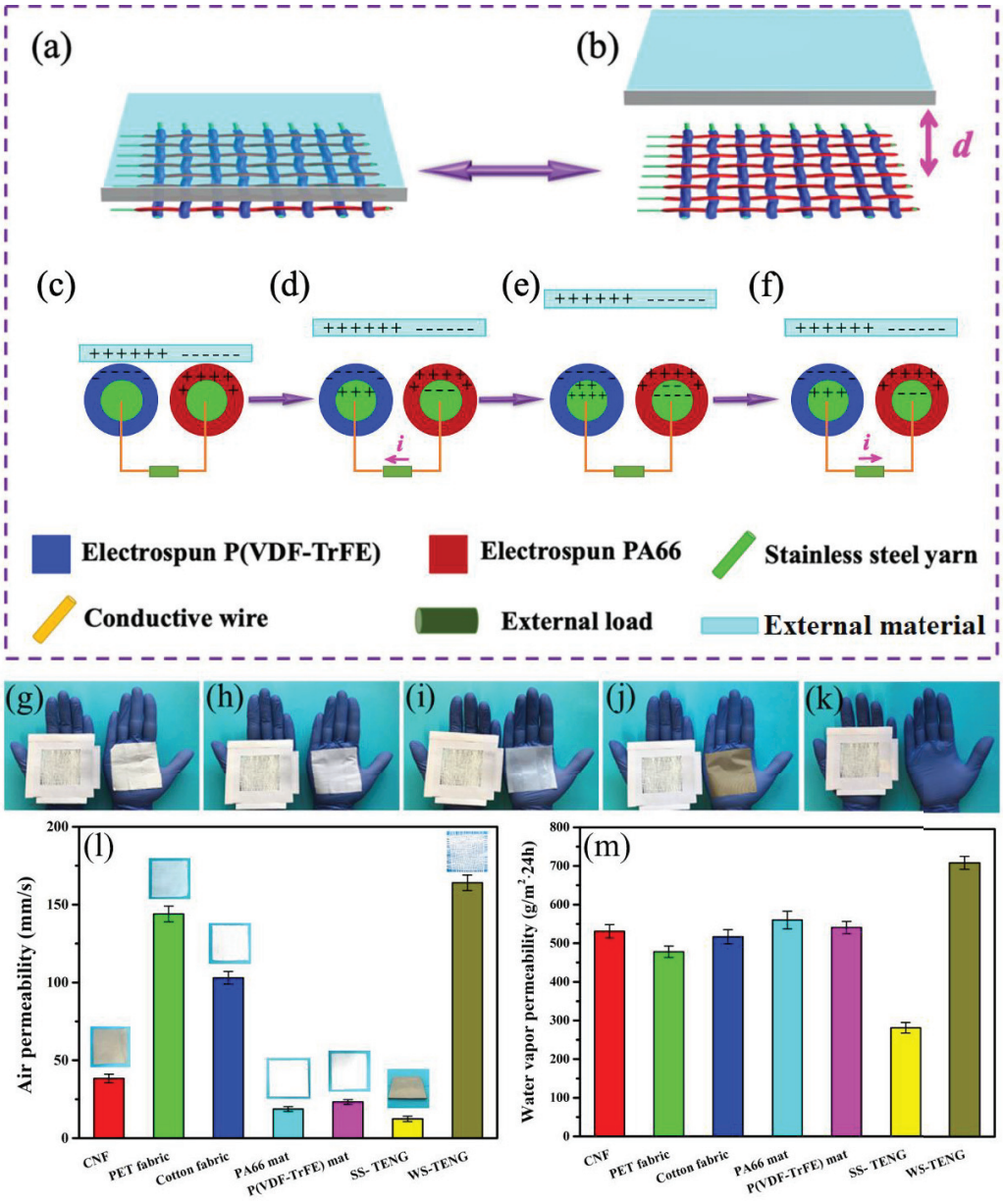

Fig. 2 (a-b) Schematic illustrations and (c-f) power generation mechanism of the WS-TENG contacted with rubber film. (g-k) Photographic images of the WS-TENG contacted with different freestanding-layer materials. (l) Air permeability and (m) water vapor permeability of the obtained WS-TENG, traditional SS-TENG and different fabrics. Insets of (l) are digital photos of each type of device/fabric with a dimension of 5 cm × 5 cm.

3.4. Output performance evaluation of the WS-TENG

The output performance of the WS-TENG in freestanding-layer mode is systematically studied. Fig.3a-b show the corresponding open-circuit voltage (V_{oc}) and

short-circuit current (I_{sc}) when using different-friction materials to flap the WS-TENG, respectively. In comparison, under a given impact force of 200 N and a frequency of 3 Hz, V_{oc} and I_{sc} of the fabricated WS-TENG were optimized to ~ 96 V and ~ 8.5 μA when using rubber as external friction material, respectively. Owing to the superior output performance, rubber was chosen as the external friction material in the following sections unless otherwise specified.

Under a given impact force of 200 N and a frequency of 3 Hz, increasing V_{oc} of 23 V, 49 V and 95 V can be obtained as the size increases from 2 × 2, 3.5 × 3.5, to 5 × 5 cm^2 (Fig.3c). Similarly, I_{sc} of the WS-TENG also increased gradually from 2.2 μA, 5.3 μA to 7.7 μA, by increasing the size from 2 × 2 cm^2 to 5 × 5 cm^2 (Fig.3d). The reason might be attributed to the larger contact areas with larger size, which could produce more charges with larger outputs. The WS-TENG with a size of 5 × 5 cm^2 was adopted in the following studies.

Due to the fact that diverse magnitudes of impact forces and frequencies could be applied to the WS-TENG in real-life application scenarios, it is essential to evaluate the influences of impact force and frequency on the electric outputs of WS-TENG. Fig. 3e-f show the V_{oc} and I_{sc} of WS-TENG at various impact forces ranging from 10 to 200 N. Measured results clearly revealed that the V_{oc} and I_{sc} of WS-TENG were gradually enhanced from 13 V and 1.7 μA to 87 V and 9 μA, by enhancing the applied impact force from 10 to 200 N, respectively. Such enhancements could be attributed to the more intimate contact between the rubber film and WS-TENG at a larger magnitude of applied impact force.

To further assess the versatility of the fabricated WS-TENG under various circumstances, the electrical output performance was measured at different impact frequencies by maintaining the external impact force at 200 N. As shown in Fig. 3g, when the impact frequency increased from 1 Hz to 5 Hz, V_{oc} increased slightly from 64 V to 96 V. The reasons can be explained as follows: Firstly, under the same applied external impact force, a higher impact frequency can stimulate the external electrons flowing in a shorter time, and thus it can boost the open-circuit voltage [57–59]. In

addition, surface charges on the surface of the friction layer would not be totally neutralized at an elevated frequency, which may also result in an increased open-circuit voltage [59]. Meanwhile, as shown in Fig. 3h, the amplitude of I_{sc} increased dramatically from 1.5 μA to 8.7 μA, which means that the increase of frequency has more significant influence on I_{sc} than V_{oc}. This could be understood that, a higher impact frequency can effectively boost charge transfer and shorten the sustained period of current peak, which leads to a higher I_{sc} amplitude. The above results clearly demonstrate that, along with the magnitude of impact force, the impact frequency also shows predominant influence on the output performance of WS-TENG.

As shown in Fig.3i-j, the dependence of output performance on external load resistances (R) has also been systematically studied. It can be seen that output voltage (V) tends to increase with increasing load resistances, while output current (I) shows an opposite trend. The instantaneous power density increased at first and then decreased with increasing load resistances from 1 KΩ to 100 MΩ. The maximum instantaneous power density arrived at 93 ± 6 mW/m^2 at a load resistance of 10 MΩ (Fig. 3j). The instantaneous power density was calculated by $W = I^2R/A$, where A is the size of the WS-TENG and is set as 5 × 5 cm^2, R is the external load resistance, and I is the corresponding output current. To evaluate the performance of the designed WS-TENG convincingly, comparisons of electric outputs between the WS-TENG and other nanofiber based TENGs in previous published papers were displayed in Table S2 (in Supporting Information). The results show that the designed WS-TENG exhibits comparable electrical output performance with multilayer structured nanofiber TENGs. However, most of the nanofiber based TENGs in the published papers cannot exhibit outstanding breathability and washability due to their intrinsic disadvantages of multilayer structures. Therefore, the WS-TENG device, which exhibits both good electrical output performance and superior air/water vapor permeability, could meet both the powering and breathable requirements of wearable TENGs during practical applications.

Considering the practical applications, it is necessary to evaluate the durability and

washability of WS-TENG. As shown in Fig.3k, after 20,000 continuous contact-separate cycles, the electric output performance of WS-TENGs was still stable without deterioration, demonstrating their excellent durability. In addition, the washability of WS-TENG device was also evaluated in repeated washing cycles. The output voltage signals generated by WS-TENG after five washing cycles shows that nearly 90% of the initial performance could be well-maintained, which ensures its washing durability in practical applications. The reasons for the decreased output performance after washing may be attributed to the slight shrinkage and relative position changes of the P(VDF-TrFE)-SSL and PA66-SSL yarns upon repeated washing cycles [60]. More specifically, a slight shrinkage of nanofiber wrapped yarns may occur during washing, which is a typical phenomenon of textile yarns after their washes. Yarn shrinkage can alter the relative position of weft and warp yarns as well as the effective contact between each other [61,62].

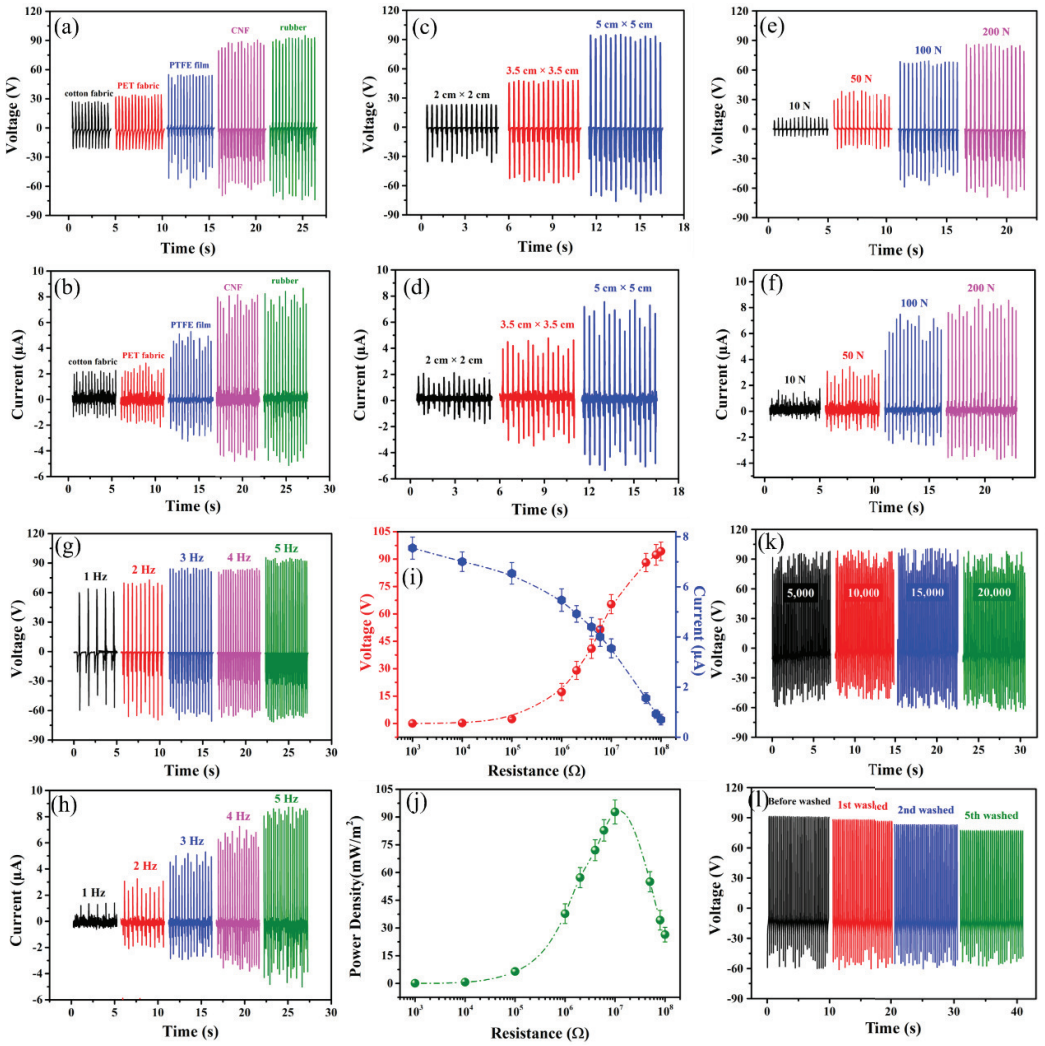

Fig. 3 (a) Open-circuit voltage and (b) short-circuit current of the WS-TENG with different friction materials. (c) Open-circuit voltage and (d) short-circuit current of the WS-TENG with different sizes. (e) Open-circuit voltage and (f) short-circuit current of the WS-TENG with different impacting forces. (g) Open-circuit voltage and (h) short-circuit current of the WS-TENG with different frequencies. (i) Dependence of the output voltage and current of the WS-TENG on load resistances. (j) Dependence of the instantaneous power density of the WS-TENG on load resistances. (k) Durability test of the WS-TENG under 20,000 continuous working cycles. (l) Electric performance of the WS-TENG before and after washing for different times.

3.5. Applications of the WS-TENG

Being flexible, breathable, washable, and easy to be triggered by various freestanding-layer materials, the fabricated WS-TENG has promising potential in diversified wearable applications. To demonstrate its flexibility and potential to harvest

biomechanical energy and monitor human motions, the WS-TENG was fixed at various positions of human body to harvest energy from human motions. For example, in the palm (Fig.4a), at the elbow joint (Fig.4c), at the lateral elbow (Fig.4e), under the arm (Fig.4g), at the knee joint (Fig.4i) and under the foot (Fig.4k). The corresponding peak-to-peak V_{oc} value can reach about 13 V (Fig.4b), 14 V(Fig.4d), 17 V (Fig.4f), 23 V(Fig.4h), 7 V (Fig.4j) and 9 V(Fig.4l), respectively. Specifically, to harvest from hands clapping, the WS-TENG was pasted in the palm of a glove, and the skin of the other hand acted as the freestanding layer during clapping (Fig.4a-b). As well known, the movement of arms and legs is also one of the most important biomechanical energy sources from human body. If WS-TENG was integrated in a coat, the energy from the elbow joint bending (Fig.4c-f) and arm swinging (Fig.4g-h) could be harvested. Here, the coats made of cotton fabric acted as the freestanding layer. When one swings arm or bend elbow joints, the contact area between the WS-TENG and the coats will change, generating an alternating-current electricity. Similarly, WS-TENG was then integrated in trousers (made of polyester fabric to act as the freestanding layer) to harvest energy from knee joint bending during walking (Fig.4i-j). In addition, the WS-TENG could also be laid under the foot to harvest energy from footsteps (Fig.4k-l), during which the sock acted as the freestanding triboelectric layer. Considering that each peak V_{oc} signal of WS-TENG corresponded to one contact-separation process, such as arm swinging or leg bending movement, the WS-TENG shows promising potential in human motion monitoring by using such peaks as sensor trigger signals, which shows the wide application prospects in personal health monitoring. To further evaluate the application potential of the WS-TENG in sensing applications, the sensing capability was studied comprehensively. As depicted in Fig.S2 (in the Supporting Information), the output voltage was plotted versus the external pressure. The results show that the WS-TENG exhibits good sensitivity of 1.824 V/kPa and 0.968 V/kPa in a wide pressure range of 0.24 to 20 kPa and 30 to 70 kPa, respectively. Compared with some previous published papers (as shown in Table S3 in the Supporting Information), the developed WS-TENG could obtain a balanced performance between a high sensitivity and a wide detection range of external pressure. More importantly, most of the TENG devices in previous

works cannot exhibit outstanding breathability and washability due to their intrinsic structures and materials. Herein, the all-fiber WS-TENG could solve the breathability and washability problems of nanofiber based devices during practical applications.

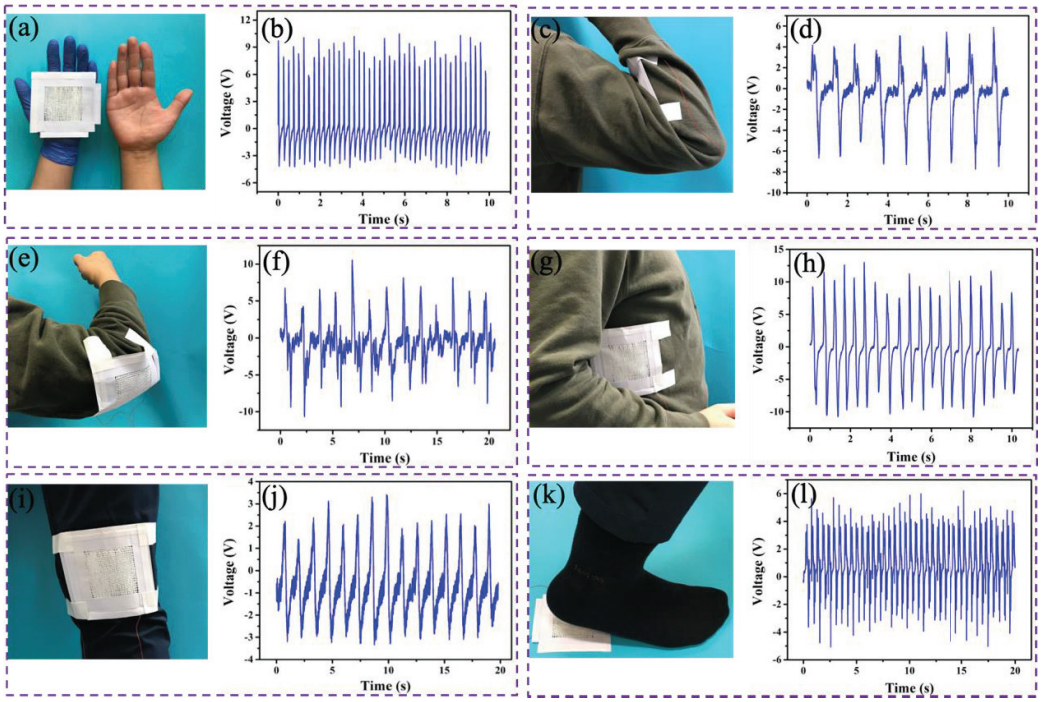

Fig. 4 Photographic images and open-circuit voltage of the WS-TENG fixed at different positions of human body. (a-b) in the palm, (c-d) at the elbow joint, (e-f) at the lateral elbow, (g-h) under the arm, (i-j) at the knee joint, (k-l) under the foot.

Furthermore, to demonstrate its application potential as a useful power source and self-powered sensor, the energy-harvesting, charging capabilities and human motion sensing potentials of WS-TENG were investigated. Through lightly flapping the WS-TENG by hand, the electric energy can directly drive 58 LEDs connected serially (Fig.5a), easily power a digital clock (Fig.5b) with a simple bridge rectifier circuit (Fig.5d). Moreover, the rectified output signals of WS-TENG could be charged into several capacitors with different capacitances. Fig.5e shows the voltage-charging curves of capacitors measured by flapping the WS-TENG. The voltages of 2 μF, 4.7 μF, 22 μF and 100 μF capacitors can reach 15.2 V, 7.8V, 3.3 V and 1.7 V in 120 s, respectively. Above results clearly reveal the WS-TENG can effectively generate electrical output under various human motions and show promising potential for

powering wearable electronics. Finally, a smart textile glove was made by stitching several WS-TENGs (area: ~2 cm^2) onto a commercial knitted cotton glove (Fig. 5c). To demonstrate its potential to detect finger movements, output voltage signals under different circumstances were investigated. Tests of bending the thumb and pressing the index finger onto a rubber pad were carried out with the smart glove and corresponding voltage signals were shown in Fig.5f and Fig.5g, respectively. When bending the thumb periodically, the WS-TENG stitched at thumb position simultaneously generated a peak-to-peak voltage of ~ 2.8 V, which could be attributed to the periodic distance change between stitched WS-TENG and the glove. When pressing the index finger onto a rubber pad at a frequency of 5 Hz, voltage signals with a peak-to-peak value of ~ 15 V were generated by corresponding WS-TENG stitched on index finger position. The measured results clearly affirm that the WS-TENG based textile sensors are capable of detecting human movements in practical applications.

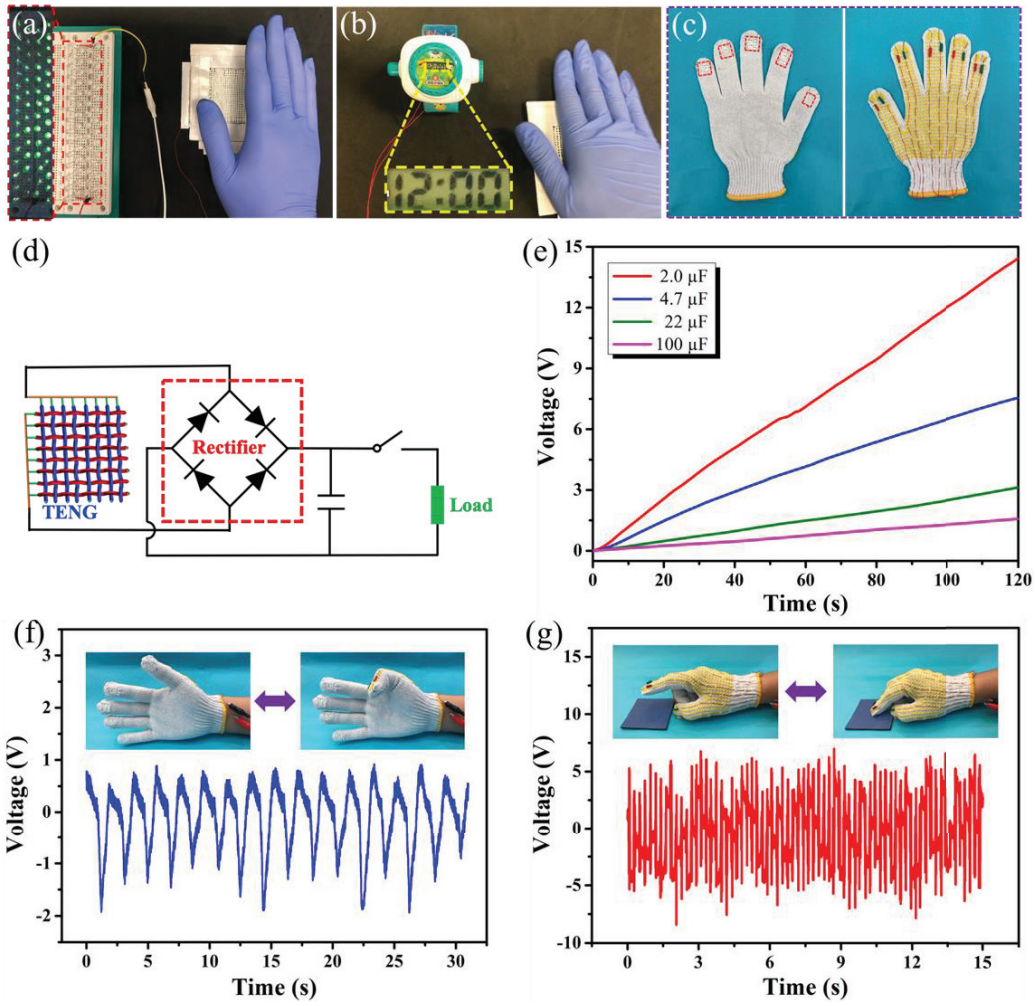

Fig. 5 Practical applications of the WS-TENG: Harvesting mechanical energy from hand flapping for (a) directly lighting up about 58 LEDs, (b) driving the electronic watch and (c) smart glove for finger motion sensing. (d) The equivalent electrical circuit of the self-powered system. (e) Charging curves of 2, 4.7, 22, 100 μF capacitors charged by the WS-TENG under flapping by a human palm. Voltage signals recorded by the smart glove when (f) bending the thumb and (g) pressing the index finger. Insets of (f) and (g) show the corresponding digital photos.

4. Conclusion

In summary, we have designed and developed a novel all-fiber triboelectric nanogenerator with a woven textile structure by using core-shell yarns with commercial stainless-steel yarns as the core and electrospun PA66 or P(VDF-TrFE) nanofibers as the shell through a simple electrospinning and scalable weaving methods. Herein, the fabricated WS-TENG exhibits the combined advantages of nanofibrous surface microstructures, all-fiber components, and interlaced-designed woven structure, which

avoid using breathless binder and protective/encapsulation layer, displaying a new approach in the fabrication of nanofiber-based WS-TENG with washability, high flexibility, desirable breathability, and excellent durability. Resultantly, the WS-TENG exhibited an obviously superior wearable performance in comparison with nanofiber-based TENG with sandwich-like structure. Specifically, under a working principle of freestanding mode, a high output open-circuit voltage with a peak-to-peak value of ~166 V and a short-circuit current of ~ 8.5 μA can be obtained from the WS-TENG with the size of 5 × 5 cm^2, corresponding to a high instantaneous power density of 93 mW/m^2 at a load resistance of about 10 MΩ. Demonstration of applications showed that the woven-structured nanofiber TENG can be well utilized to harvest biomechanical energy from human motions and are expected to be further employed in self-powered devices.

Conflict of interest

The authors declare no competing financial interest.

Acknowledgements

The authors acknowledge The Hong Kong Polytechnic University (G-YBV2) for funding supports of this work. Guan Xiaoyang would also like to thank The Hong Kong Polytechnic University for providing him with a postgraduate scholarship.

References

[1] E. Song, J. Li, S.M. Won, W. Bai, J.A. Rogers, Materials for flexible bioelectronic systems as chronic neural interfaces, Nat. Mater. 19 (2020) 590–603. https://doi.org/10.1038/s41563-020-0679-7.

[2] M. Kaltenbrunner, T. Sekitani, J. Reeder, T. Yokota, K. Kuribara, T. Tokuhara, M. Drack, R. Schwödiauer, I. Graz, S. Bauer-Gogonea, S. Bauer, T. Someya, An ultra-lightweight design for imperceptible plastic electronics, Nature. 499 (2013) 458–463. https://doi.org/10.1038/nature12314.

[3] Q. Fu, Y. Chen, M. Sorieul, Wood-Based Flexible Electronics, ACS Nano. 14

(2020) 3528–3538. https://doi.org/10.1021/acsnano.9b09817.

[4] R. Ramya, G. Saravanakumar, S. Ravi, Energy harvesting in wireless sensor networks, Adv. Intell. Syst. Comput. 394 (2016) 841–853. https://doi.org/10.1007/978-81-322-2656-7_76.

[5] F. Wen, H. Wang, T. He, Q. Shi, Z. Sun, M. Zhu, Z. Zhang, Z. Cao, Y. Dai, T. Zhang, C. Lee, Battery-free short-range self-powered wireless sensor network (SS-WSN) using TENG based direct sensory transmission (TDST) mechanism, Nano Energy. 67 (2020). https://doi.org/10.1016/j.nanoen.2019.104266.

[6] X. Fan, J. He, J. Mu, J. Qian, N. Zhang, C. Yang, X. Hou, W. Geng, X. Wang, X. Chou, Triboelectric-electromagnetic hybrid nanogenerator driven by wind for self-powered wireless transmission in Internet of Things and self-powered wind speed sensor, Nano Energy. 68 (2020). https://doi.org/10.1016/j.nanoen.2019.104319.

[7] G.H. Gelinck, H.E.A. Huitema, E. Van Veenendaal, E. Cantatore, L. Schrijnemakers, J.B.P.H. Van Der Putten, T.C.T. Geuns, M. Beenhakkers, J.B. Giesbers, B.H. Huisman, E.J. Meijer, E.M. Benito, F.J. Touwslager, A.W. Marsman, B.J.E. Van Rens, D.M. De Leeuw, Flexible active-matrix displays and shift registers based on solution-processed organic transistors, Nat. Mater. 3 (2004) 106–110. https://doi.org/10.1038/nmat1061.

[8] H. Fukagawa, T. Sasaki, T. Tsuzuki, Y. Nakajima, T. Takei, G. Motomura, M. Hasegawa, K. Morii, T. Shimizu, Long-Lived Flexible Displays Employing Efficient and Stable Inverted Organic Light-Emitting Diodes, Adv. Mater. 30 (2018) 1–7. https://doi.org/10.1002/adma.201706768.

[9] D. Zhang, T. Huang, L. Duan, Emerging Self-Emissive Technologies for Flexible Displays, Adv. Mater. 32 (2020) 1–42. https://doi.org/10.1002/adma.201902391.

[10] T.Q. Trung, N.E. Lee, Flexible and Stretchable Physical Sensor Integrated Platforms for Wearable Human-Activity Monitoringand Personal Healthcare, Adv. Mater. 28 (2016) 4338–4372. https://doi.org/10.1002/adma.201504244.

[11] N. Zhang, Y. Li, S. Xiang, W. Guo, H. Zhang, C. Tao, S. Yang, X. Fan,

Imperceptible sleep monitoring bedding for remote sleep healthcare and early disease diagnosis, Nano Energy. 72 (2020). https://doi.org/10.1016/j.nanoen.2020.104664.

[12] S. Ji, C. Wan, T. Wang, Q. Li, G. Chen, J. Wang, Z. Liu, H. Yang, X. Liu, X. Chen, Water-Resistant Conformal Hybrid Electrodes for Aquatic Endurable Electrocardiographic Monitoring, Adv. Mater. (2020). https://doi.org/10.1002/adma.202001496.

[13] Q. Shi, Z. Zhang, T. Chen, C. Lee, Minimalist and multi-functional human machine interface (HMI) using a flexible wearable triboelectric patch, Nano Energy. 62 (2019) 355–366. https://doi.org/10.1016/j.nanoen.2019.05.033.

[14] B. Zhang, Y. Tang, R. Dai, H. Wang, X. Sun, C. Qin, Z. Pan, E. Liang, Y. Mao, Breath-based human–machine interaction system using triboelectric nanogenerator, Nano Energy. 64 (2019). https://doi.org/10.1016/j.nanoen.2019.103953.

[15] X. Zhao, Z. Kang, Q. Liao, Z. Zhang, M. Ma, Q. Zhang, Y. Zhang, Ultralight, self-powered and self-adaptive motion sensor based on triboelectric nanogenerator for perceptual layer application in Internet of things, Nano Energy. 48 (2018) 312–319. https://doi.org/10.1016/j.nanoen.2018.03.072.

[16] Z.L. Wang, Entropy theory of distributed energy for internet of things, Nano Energy. 58 (2019) 669–672. https://doi.org/10.1016/j.nanoen.2019.02.012.

[17] K. Zhou, Y. Zhao, X. Sun, Z. Yuan, G. Zheng, K. Dai, L. Mi, C. Pan, C. Liu, C. Shen, Ultra-stretchable triboelectric nanogenerator as high-sensitive and self-powered electronic skins for energy harvesting and tactile sensing, Nano Energy. 70 (2020). https://doi.org/10.1016/j.nanoen.2020.104546.

[18] S. Huang, B. Zhang, Z. Shao, L. He, Q. Zhang, J. Jie, X. Zhang, Ultraminiaturized Stretchable Strain Sensors Based on Single Silicon Nanowires for Imperceptible Electronic Skins, Nano Lett. 20 (2020) 2478–2485. https://doi.org/10.1021/acs.nanolett.9b05217.

[19] S. Liu, S. Wang, S. Xuan, S. Zhang, X. Fan, H. Jiang, P. Song, X. Gong, Highly Flexible Multilayered e-Skins for Thermal-Magnetic-Mechanical Triple Sensors

and Intelligent Grippers, ACS Appl. Mater. Interfaces. 12 (2020) 15675–15685. https://doi.org/10.1021/acsami.9b23547.

[20] X. Cheng, L. Miao, Y. Song, Z. Su, H. Chen, X. Chen, J. Zhang, H. Zhang, High efficiency power management and charge boosting strategy for a triboelectric nanogenerator, Nano Energy. 38 (2017) 438–446. https://doi.org/10.1016/j.nanoen.2017.05.063.

[21] Y. Chen, B. Xu, J. Gong, J. Wen, T. Hua, C.W. Kan, J. Deng, Design of High-Performance Wearable Energy and Sensor Electronics from Fiber Materials, ACS Appl. Mater. Interfaces. 11 (2019) 2120–2129. https://doi.org/10.1021/acsami.8b16167.

[22] K. Dong, Y.C. Wang, J. Deng, Y. Dai, S.L. Zhang, H. Zou, B. Gu, B. Sun, Z.L. Wang, A Highly Stretchable and Washable All-Yarn-Based Self-Charging Knitting Power Textile Composed of Fiber Triboelectric Nanogenerators and Supercapacitors, ACS Nano. 11 (2017) 9490–9499. https://doi.org/10.1021/acsnano.7b05317.

[23] J. Wang, S. Li, F. Yi, Y. Zi, J. Lin, X. Wang, Y. Xu, Z.L. Wang, Sustainably powering wearable electronics solely by biomechanical energy, Nat. Commun. 7 (2016) 1–8. https://doi.org/10.1038/ncomms12744.

[24] J. Gong, B. Xu, X. Guan, Y. Chen, S. Li, J. Feng, Towards truly wearable energy harvesters with full structural integrity of fiber materials, Nano Energy. 58 (2019) 365–374. https://doi.org/10.1016/j.nanoen.2019.01.056.

[25] X. Guan, B. Xu, J. Gong, Hierarchically architected polydopamine modified BaTiO3@P(VDF-TrFE) nanocomposite fiber mats for flexible piezoelectric nanogenerators and self-powered sensors, Nano Energy. 70 (2020). https://doi.org/10.1016/j.nanoen.2020.104516.

[26] P. Maharjan, T. Bhatta, M. Salauddin Rasel, M. Salauddin, M. Toyabur Rahman, J.Y. Park, High-performance cycloid inspired wearable electromagnetic energy harvester for scavenging human motion energy, Appl. Energy. 256 (2019) 1–10. https://doi.org/10.1016/j.apenergy.2019.113987.

[27] Z.L. Wang, On Maxwell's displacement current for energy and sensors: the

origin of nanogenerators, Mater. Today. 20 (2017) 74–82. https://doi.org/10.1016/j.mattod.2016.12.001.

[28] Y. Jie, Q. Jiang, Y. Zhang, N. Wang, X. Cao, A structural bionic design: From electric organs to systematic triboelectric generators, Nano Energy. 27 (2016) 554–560. https://doi.org/10.1016/j.nanoen.2016.07.028.

[29] Y. Jie, H. Zhu, X. Cao, Y. Zhang, N. Wang, L. Zhang, Z.L. Wang, One-Piece Triboelectric Nanosensor for Self-Triggered Alarm System and Latent Fingerprint Detection, ACS Nano. 10 (2016) 10366–10372. https://doi.org/10.1021/acsnano.6b06100.

[30] X. Cao, Y. Jie, N. Wang, Z.L. Wang, Triboelectric Nanogenerators Driven Self-Powered Electrochemical Processes for Energy and Environmental Science, Adv. Energy Mater. 6 (2016). https://doi.org/10.1002/aenm.201600665.

[31] A. Proto, M. Penhaker, S. Conforto, M. Schmid, Nanogenerators for Human Body Energy Harvesting, Trends Biotechnol. 35 (2017) 610–624. https://doi.org/10.1016/j.tibtech.2017.04.005.

[32] T. Jing, B. Xu, X. Guan, Y. Yang, M. Wu, C. Jiang, Liquid-Filling Polydimethylsiloxane Composites with Enhanced Triboelectric Performance for Flexible Nanogenerators, Macromol. Mater. Eng. 305 (2020). https://doi.org/10.1002/mame.202000275.

[33] Y. Yang, T. Jing, B. Xu, Self-Assembly of Porous Microstructured Polydimethylsiloxane Films for Wearable Triboelectric Nanogenerators, Macromol. Mater. Eng. 305 (2020). https://doi.org/10.1002/mame.202000276.

[34] F.R. Fan, Z.Q. Tian, Z. Lin Wang, Flexible triboelectric generator, Nano Energy. 1 (2012) 328–334. https://doi.org/10.1016/j.nanoen.2012.01.004.

[35] F.R. Fan, L. Lin, G. Zhu, W. Wu, R. Zhang, Z.L. Wang, Transparent triboelectric nanogenerators and self-powered pressure sensors based on micropatterned plastic films, Nano Lett. 12 (2012) 3109–3114. https://doi.org/10.1021/nl300988z.

[36] J. Xiong, P. Cui, X. Chen, J. Wang, K. Parida, M.F. Lin, P.S. Lee, Skin-touch-actuated textile-based triboelectric nanogenerator with black phosphorus for

durable biomechanical energy harvesting, Nat. Commun. 9 (2018) 1–9. https://doi.org/10.1038/s41467-018-06759-0.

[37] T. Jing, B. Xu, Y. Yang, Liquid doping materials as micro-carrier of functional molecules for functionalization of triboelectric materials and flexible triboelectric nanogenerators for energy harvesting and gesture detection, Nano Energy. 74 (2020). https://doi.org/10.1016/j.nanoen.2020.104856.

[38] S. Niu, X. Wang, F. Yi, Y.S. Zhou, Z.L. Wang, A universal self-charging system driven by random biomechanical energy for sustainable operation of mobile electronics, Nat. Commun. 6 (2015). https://doi.org/10.1038/ncomms9975.

[39] Z. Tian, J. He, X. Chen, Z. Zhang, T. Wen, C. Zhai, J. Han, J. Mu, X. Hou, X. Chou, C. Xue, Performance-boosted triboelectric textile for harvesting human motion energy, Nano Energy. 39 (2017) 562–570. https://doi.org/10.1016/j.nanoen.2017.06.018.

[40] J. Gong, B. Xu, X. Tao, Breath Figure Micromolding Approach for Regulating the Microstructures of Polymeric Films for Triboelectric Nanogenerators, ACS Appl. Mater. Interfaces. 9 (2017) 4988–4997. https://doi.org/10.1021/acsami.6b14729.

[41] X. Guan, J. Gong, B. Xu, Three-Dimensional Conformal Porous Microstructural Engineering of Textile Substrates with Customized Functions of Brick Materials and Inherent Advantages of Textiles, ACS Appl. Mater. Interfaces. 12 (2020) 17967–17978. https://doi.org/10.1021/acsami.0c01557.

[42] W. Yang, X. Wang, H. Li, J. Wu, Y. Hu, Z. Li, H. Liu, Fundamental research on the effective contact area of micro-/nano-textured surface in triboelectric nanogenerator, Nano Energy. 57 (2019) 41–47. https://doi.org/10.1016/j.nanoen.2018.12.029.

[43] H.Y. Li, L. Su, S.Y. Kuang, C.F. Pan, G. Zhu, Z.L. Wang, Significant Enhancement of Triboelectric Charge Density by Fluorinated Surface Modification in Nanoscale for Converting Mechanical Energy, Adv. Funct. Mater. 25 (2015) 5691–5697. https://doi.org/10.1002/adfm.201502318.

[44] J. Gong, B. Xu, Y. Yang, M. Wu, B. Yang, An Adhesive Surface Enables High-

Performance Mechanical Energy Harvesting with Unique Frequency-Insensitive and Pressure-Enhanced Output Characteristics, Adv. Mater. 32 (2020) 1–7. https://doi.org/10.1002/adma.201907948.

[45] W. Kim, T. Okada, H.W. Park, J. Kim, S. Kim, S.W. Kim, S. Samukawa, D. Choi, Surface modification of triboelectric materials by neutral beams, J. Mater. Chem. A. 7 (2019) 25066–25077. https://doi.org/10.1039/c9ta09990e.

[46] L. Han, M. Peng, Z. Wen, Y. Liu, Y. Zhang, Q. Zhu, H. Lei, S. Liu, L. Zheng, X. Sun, H. Li, Self-driven photodetection based on impedance matching effect between a triboelectric nanogenerator and a MoS2 nanosheets photodetector, Nano Energy. 59 (2019) 492–499. https://doi.org/10.1016/j.nanoen.2019.02.072.

[47] X.S. Zhang, M. Su, J. Brugger, B. Kim, Penciling a triboelectric nanogenerator on paper for autonomous power MEMS applications, Nano Energy. 33 (2017) 393–401. https://doi.org/10.1016/j.nanoen.2017.01.053.

[48] J. Huang, X. Fu, G. Liu, S. Xu, X. Li, C. Zhang, L. Jiang, Micro/nano-structures-enhanced triboelectric nanogenerators by femtosecond laser direct writing, Nano Energy. 62 (2019) 638–644. https://doi.org/10.1016/j.nanoen.2019.05.081.

[49] W. Shang, G.Q. Gu, F. Yang, L. Zhao, G. Cheng, Z.L. Du, Z.L. Wang, A Sliding-Mode Triboelectric Nanogenerator with Chemical Group Grated Structure by Shadow Mask Reactive Ion Etching, ACS Nano. 11 (2017) 8796–8803. https://doi.org/10.1021/acsnano.7b02866.

[50] J. Xue, T. Wu, Y. Dai, Y. Xia, Electrospinning and electrospun nanofibers: Methods, materials, and applications, Chem. Rev. 119 (2019) 5298–5415. https://doi.org/10.1021/acs.chemrev.8b00593.

[51] X. Guan, G. Zheng, K. Dai, C. Liu, X. Yan, C. Shen, Z. Guo, Carbon Nanotubes-Adsorbed Electrospun PA66 Nanofiber Bundles with Improved Conductivity and Robust Flexibility, ACS Appl. Mater. Interfaces. 8 (2016) 14150–14159. https://doi.org/10.1021/acsami.6b02888.

[52] Z. Zhang, W. Gong, Z. Bai, D. Wang, Y. Xu, Z. Li, J. Guo, L.S. Turng, Oxygen-Rich Polymers as Highly Effective Positive Tribomaterials for Mechanical Energy Harvesting, ACS Nano. 13 (2019) 12787–12797.

https://doi.org/10.1021/acsnano.9b04911.

[53] T. Huang, C. Wang, H. Yu, H. Wang, Q. Zhang, M. Zhu, Human walking-driven wearable all-fiber triboelectric nanogenerator containing electrospun polyvinylidene fluoride piezoelectric nanofibers, Nano Energy. 14 (2014) 226–235. https://doi.org/10.1016/j.nanoen.2015.01.038.

[54] P. Zhao, N. Soin, K. Prashanthi, J. Chen, S. Dong, E. Zhou, Z. Zhu, A.A. Narasimulu, C.D. Montemagno, L. Yu, J. Luo, Emulsion Electrospinning of Polytetrafluoroethylene (PTFE) Nanofibrous Membranes for High-Performance Triboelectric Nanogenerators, ACS Appl. Mater. Interfaces. 10 (2018) 5880–5891. https://doi.org/10.1021/acsami.7b18442.

[55] B.U. Ye, B.J. Kim, J. Ryu, J.Y. Lee, J.M. Baik, K. Hong, Electrospun ion gel nanofibers for flexible triboelectric nanogenerator: electrochemical effect on output power, Nanoscale. 7 (2015) 16189–16194. https://doi.org/10.1039/c5nr02602d.

[56] Z. Li, J. Shen, I. Abdalla, J. Yu, B. Ding, Nanofibrous membrane constructed wearable triboelectric nanogenerator for high performance biomechanical energy harvesting, Nano Energy. 36 (2017) 341–348. https://doi.org/10.1016/j.nanoen.2017.04.035.

[57] Q. Ye, Y. Wu, Y. Qi, L. Shi, S. Huang, L. Zhang, M. Li, W. Li, X. Zeng, H. Wo, X. Wang, S. Dong, S. Ramakrishna, J. Luo, Effects of liquid metal particles on performance of triboelectric nanogenerator with electrospun polyacrylonitrile fiber films, Nano Energy. 61 (2019) 381–388. https://doi.org/10.1016/j.nanoen.2019.04.075.

[58] J. Shen, Z. Li, J. Yu, B. Ding, Humidity-resisting triboelectric nanogenerator for high performance biomechanical energy harvesting, Nano Energy. 40 (2017) 282–288. https://doi.org/10.1016/j.nanoen.2017.08.035.

[59] X.S. Zhang, M. Di Han, R.X. Wang, F.Y. Zhu, Z.H. Li, W. Wang, H.X. Zhang, Frequency-multiplication high-output triboelectric nanogenerator for sustainably powering biomedical microsystems, Nano Lett. 13 (2013) 1168–1172. https://doi.org/10.1021/nl3045684.

[60] Z. Zhao, Q. Huang, C. Yan, Y. Liu, X. Zeng, X. Wei, Y. Hu, Z. Zheng, Machine-washable and breathable pressure sensors based on triboelectric nanogenerators enabled by textile technologies, Nano Energy. 70 (2020) 104528. https://doi.org/10.1016/j.nanoen.2020.104528.

[61] W. Yang, R. Cao, X. Zhang, H. Li, C. Li, Air-Permeable and Washable Paper–Based Triboelectric Nanogenerator Based on Highly Flexible and Robust Paper Electrodes, Adv. Mater. Technol. 3 (2018) 1–9. https://doi.org/10.1002/admt.201800178.

[62] Z. Zhao, C. Yan, Z. Liu, X. Fu, L.-M. Peng, Y. Hu, Z. Zheng, Machine-Washable Textile Triboelectric Nanogenerators for Effective Human Respiratory Monitoring through Loom Weaving of Metallic Yarns, Adv. Mater. 28 (2016) 10267–10274. https://doi.org/10.1002/adma.201603679.